

## APPLICATION OF A GLOBAL/LOCAL ANALYSIS TO STUDY SIZE EFFECT IN CONCRETE

C. OLIVER-LEBLOND\*, A. DELAPLACE† AND F. RAGUENEAU\*

\*LMT-Cachan (ENS Cachan/CNRS/Université Paris 6/UniverSud Paris)  
61 avenue du Président Wilson, 94230 Cachan, France  
e-mail: oliver@lmt.ens-cachan.fr, ragueneau@lmt.ens-cachan.fr

†Lafarge Centre de Recherche  
95 rue de Montmurier, 38291 Saint Quentin Fallavier, France  
e-mail: arnaud.delaplace@pole-technologique.lafarge.com

**Key words:** Size effect, Damage, Cracking, Discrete Element Method, Continuous Approach.

**Abstract.** A global/local method, or sub-modelling method, has been developed to obtain a fine description of cracking in concrete specimen. A discrete-element model is used to re-analyse at a local scale the damage zone obtained after the finite-element analysis of the global specimen. This strategy is applied to study the influence of size effect on cracking of plain concrete. The numerical results are compared to available experimental results obtained with the Digital Image Correlation method.

### 1 INTRODUCTION

Nowadays, experimental campaigns on large concrete structures are very rare because their cost is still prohibitive. Therefore, numerical models are mostly validated and calibrated according to results provided by small laboratory tests. The extrapolation of the laboratory results to large structures should follow the size effect theory. The influence of size effect on strength has been investigated for several years [1]. Recent experimental studies [2] have also put in evidence the influence of size effect on crack features propagation, length and opening. A global/local analysis [3] is used to study the size effect. Indeed, this computational strategy aims at quantifying cracking at the structural scale. First, a continuous damage model is used to perform a full calculation at the global scale. This damage model which takes into account damage coupled to permanent strain and hysteresis is able to produce some information about

the non-linear behaviour (load redistribution, stiffness decrease, dissipated energy) but not about the cracking. Information about cracking (tortuosity, heterogeneities and openings) is extracted by using a reanalysis of the damaged zones at the local scale with a discrete element model [4]. The global/local technique proposed is non-intrusive and decoupled so the reanalysis can be seen as a post-treatment. Plus, the two-scale analysis uses each numerical model within its more efficient level. This presentation aims at comparing the numerical results obtained from the proposed strategy with experimental results from three-points bending tests exhibiting size effect. The relevancy of the two scale approach is emphasized thanks to experimental field measurements around the crack path. The parameters identification strategies of the two levels of modelling based on an equivalent energy dissipation rate will be also addressed.

## 2 THE GLOBAL MODEL

The model used at the global scale is a finite-element model coupling elasticity, isotropic damage and internal sliding (see [5]). The state potential is given by the Helmholtz free energy:

$$\begin{aligned} \rho\Psi = & \frac{\kappa}{6}((1-d) \langle \epsilon_{kk} \rangle_+^2 + \langle \epsilon_{kk} \rangle_-^2) \\ & + \mu(1-d)\epsilon_{ij}^d\epsilon_{ij}^d + \mu d(\epsilon_{ij}^d - \epsilon_{ij}^\pi)(\epsilon_{ij}^d - \epsilon_{ij}^\pi) \\ & + \frac{\gamma}{2}\alpha_{ij}\alpha_{ij} + H(z) \end{aligned} \quad (1)$$

where  $\rho$  is the material density,  $\Psi$  the Helmholtz free energy,  $d$  the scalar damage variable ranging from 0 (virgin material) to 1 (failed material),  $\epsilon_{ij}$  the total strains second-order tensor,  $\epsilon_{ij}^\pi$  the internal sliding second-order tensor,  $\alpha_{ij}$  the kinematic hardening second-order tensor,  $z$  the scalar isotropic hardening variable,  $H$  the consolidation function,  $\kappa$  the bulk coefficient,  $\mu$  the shear modulus and  $\gamma$  the kinematic hardening parameter that has to be identified from measurements.  $\langle . \rangle_+$  and  $\langle . \rangle_-$  stand for the positive part and the negative part of  $(.)$  respectively.  $(.)^d$  is the deviatoric part of  $(.)$  defined as  $(.)^d = (.) - \frac{1}{3}(.)_{kk}$ .

This model can describe the local mechanisms related to concrete such as the asymmetry between the tensile behaviour and the compressive behaviour, the inelastic strains and the unilateral effect. Moreover, it is robust and can handle large-scale computation.

However, this model requires the introduction of a characteristic length to prevent the occurrence of spurious mesh dependency related to strain softening. Here, the regularization of the problem is ensured by means of the well-known non-local technique [8]. The energy release rate is averaged in  $\Omega(\mathbf{x}, l_c)$ , where  $\mathbf{x}$  and  $l_c$  respectively stand for the current Gauss point and the characteristic length and is therefore expressed as:

$$\tilde{Y}(\mathbf{x}) = \frac{\int_{\Omega(\mathbf{x}, l_c)} \bar{Y}(\mathbf{s}) \Lambda(\mathbf{x} - \mathbf{s}) d\mathbf{s}}{\int_{\Omega(\mathbf{x}, l_c)} \Lambda(\mathbf{x} - \mathbf{s}) d\mathbf{s}} \quad (2)$$

where  $\Lambda$  is the Gaussian distribution. This regularization tends to smooth the discontinuity and thus makes the study of the cracks complex.

## 3 THE LOCAL MODEL

The local model is a discrete-element model based on a particle assembly, computed from a Voronoi tessellation. Neighbour particles are linked together by elastic Euler-Bernoulli beams representing cohesion forces (lattice model). The non-linear behaviour of the material is obtained by considering that the beams obey a brittle behaviour.

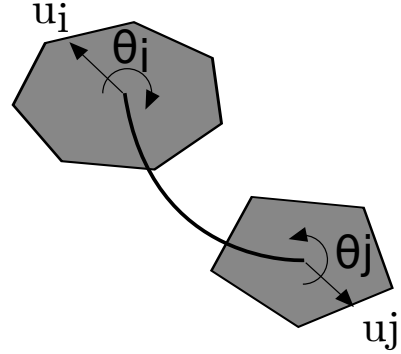


Figure 1: Euler-Bernoulli beam in a deformed state.

The breaking threshold  $P_{ij}$  of the beam  $i - j$  depends on the beam strain  $\epsilon_{ij}$  and on the rotations of the particles linked by the beam  $\theta_i$  and  $\theta_j$  (see figure 1). It is written as:

$$P_{ij} = \left( \frac{\epsilon_{ij}}{\epsilon_{ij}^{cr}} \right)^2 + \frac{|\theta_i - \theta_j|}{\theta_{ij}^{cr}} > 1 \quad (3)$$

The critical strain  $\epsilon_{ij}^{cr}$  and the critical rotation  $\theta_{ij}^{cr}$  of the beam  $i - j$  are assigned to the beam  $i - j$  using a random number generator according to the Weibull distribution, as proposed by [6].

This model gives complete information about the macro-cracking (initiation, propagation, opening, length) and the micro-cracking. Unfortunately, large-scale computation are impractical because the time needed to complete them is prohibitive.

More details about this model can be found in [4].

## 4 THE NUMERICAL STRATEGY

The method used here is inspired by the sub-modelling techniques [7]. This is a non-intrusive method which only uses available in-

put and output (nodal displacements). It is composed of the following steps:

- **Global analysis** of the whole structure with a non-linear finite element model including damage;
- **Identification and cutting of the ROI (Region of Interest)**, which is the region of damage concentration;
- **Extraction and interpolation of the displacements** from the global mesh to the local mesh;
- **Local analysis** of the ROI with a discrete element model.

The local forces are not used to perform a correction of the global computation with the local results. Indeed, the local re-analysis is a post-processing tool which gives complementary information on the kinematic of the cracks.

## 5 APPLICATION

The global/local analysis presented above has been applied to size effect tests on three-points bending concrete beams.

### 5.1 Experimental study

The beams used in [2] have a rectangular cross section of height  $d$  and thickness  $b$ .

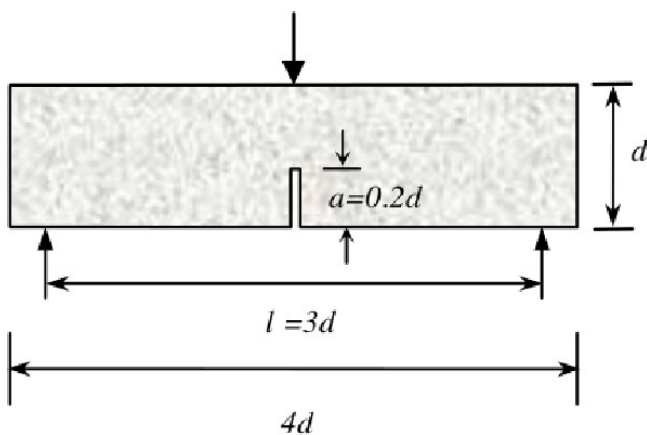


Figure 2: Geometry of the beams [2].

The span of the beam is  $l = 3d$ . The beams are notched at midspan with a length of  $a = 0.2d$ . The geometry of the beams is given

on figure 2. Three sizes of geometrically similar beams are studied: D1 ( $d = 100mm$ ), D2 ( $d = 200mm$ ) and D3 ( $d = 400mm$ ). The thickness is constant at  $b = 100mm$  for all the sizes. At least three beams have been tested for each size.

The Digital Image Correlation (DIC) technique was used to obtain experimental information on the cracking. Indeed, the fine description of the experimental displacement field through DIC allows the extraction of the crack geometry, tip and opening. Moreover, the computation of the experimental strain field gives the strain localization zone corresponding to the micro-cracking area.

The material parameters are summarized in table 1.

Table 1: Material parameters

Young's modulus	GPa	$E$	38
Poisson's coefficient	-	$\nu$	0.21
Tensile strength	MPa	$f_t$	3.5

### 5.2 Numerical study

#### 5.2.1 Meshes and loading conditions

The global mesh used for the analysis of the D1 beam is presented on top of figure 3. The ROI, centered on the damage zone, is delimited by a red square.

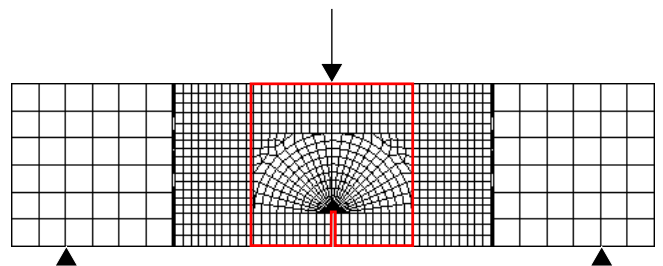


Figure 3: Global mesh

The local mesh of the ROI for the D1 specimen is presented on bottom of figure 4. Displacements extracted of the global computation are applied on the black boundaries of the local mesh while the red boundaries are kept free.

The global and the local mesh densities are constant for each size of the beam.

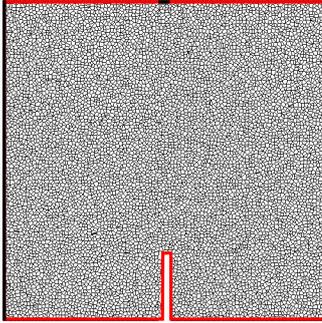


Figure 4: Local mesh

### 5.2.2 Models parameters identification

The calibration of the nonlocal global model follows the procedure proposed by Le Bellégo [9]. The calibration relies on inverse analysis and an optimisation algorithm. The complete load deflection curves for each size of beam are used in order to capture correctly the size effect. The global model parameters identified with this method are given on table 2.

Table 2: Material parameters for the global model

Tensile brittleness	$\text{J}^{-1} \cdot \text{m}^3$	$A_{Dir}$	$4.6 \cdot 10^{-3}$
Comp. brittleness	$\text{J}^{-1} \cdot \text{m}^3$	$A_{Ind}$	$3.5 \cdot 10^{-4}$
Kinematic hardening 1	Pa	$\gamma$	$2.0 \cdot 10^7$
Kinematic hardening 2	$\text{Pa}^{-1}$	$a$	$7.0 \cdot 10^{-7}$
Characteristic length	mm	$l_c$	20

The local model parameters are calibrated according to the methods presented in [4] and [3]. Because the lattice models are naturally able to capture the size effect, no additional feature has been added to these methods. The local parameters are summarized in table 3.

Table 3: Material parameters for the local model beams

Young's modulus	GPa	$E$	40
Inertia ratio	-	$\alpha$	0.83
Rotation threshold	-	$\theta_{cr}$	$5 \cdot 10^{-3}$
Scale parameter	-	$\lambda_{\epsilon_{cr}}$	$3.25 \cdot 10^{-4}$
Shape parameter	-	$k_{\epsilon_{cr}}$	0.6
Min. strain threshold	-	$\epsilon_{cr,min}$	$1.1 \cdot 10^{-4}$

### 5.2.3 Numerical results

The effect of the beam size on the load-CMOD (Crack Mouth Opening Displacement) response is presented on figure 5. The numerical results obtained with the global model are in agreement with the experimental results.

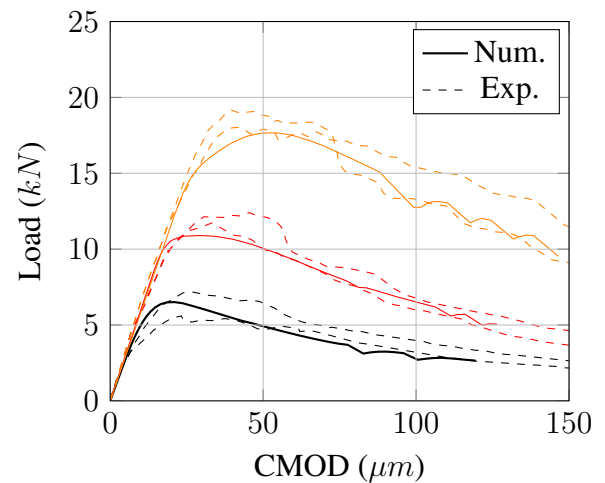


Figure 5: Load-CMOD curves (D1: black, D2: red and D3: orange)

Figure 6 shows a comparison between the measured and calculated size effect for concrete beams. In addition, the results of the size effect law by Bazant [1] are printed. According to this size effect law, the nominal strength is expressed as:

$$\sigma_n = \frac{B f_t}{\sqrt{1 - (D/D_0)}} \quad (4)$$

where  $f_t$  is the tensile strength,  $B$  a dimensionless parameter depending of the structure geometry,  $D$  the beam height and  $D_0$  the transitional

size. The experimental and numerical beam nominal strength shows strong size dependence and match well the size effect law.

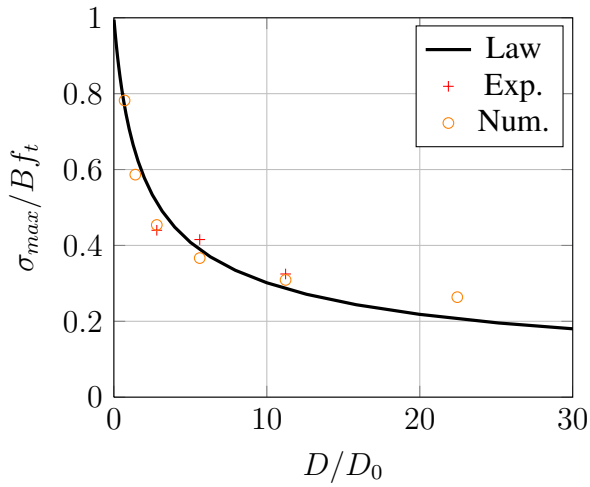


Figure 6: Normalized diagram of the size effect results

The comparison of the amount of dissipated energy inside the ROI during the global computation and the local computation gives us an appreciation of the agreement between the global analysis and the local re-analysis (see figure 7).

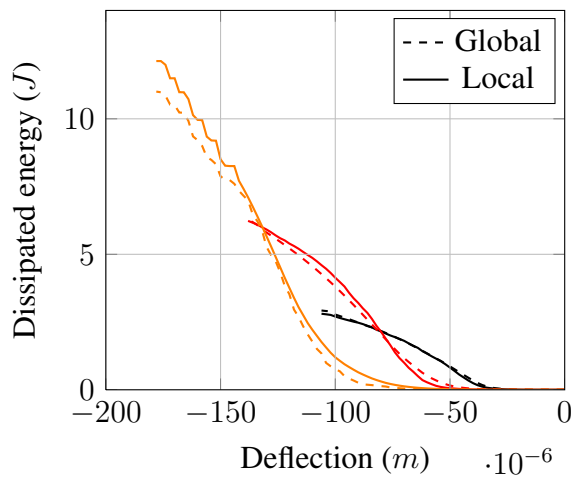


Figure 7: Comparison of the global and the local dissipated energy-deflection responses (D1: black, D2: red and D3: orange)

Finally, the results in term of cracking extracted from the local re-analysis are compared to the experimental results on figure 8 and 9. A gap is observed between the experimental crack

features (length and opening) and the numerical ones but is in accordance with the experimental variation of  $\pm 5\mu m$ .

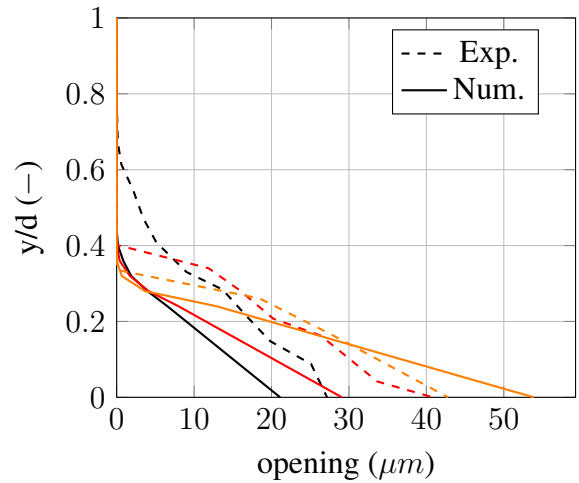


Figure 8: Crack opening profile at peak (D1: black, D2: red and D3: orange)

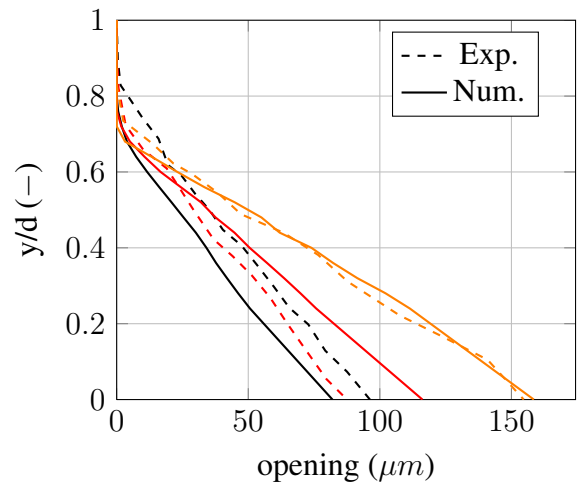


Figure 9: Crack opening profile at 60% post-peak (D1: black, D2: red and D3: orange)

It has been observed, both experimentally and numerically, that crack lengths and crack openings increase non-proportionally to the size. It does not follow Bazant's size effect law either.

## 6 CONCLUSIONS

A numerical strategy to obtain a fine description of cracking in plain concrete specimen

has been applied to size effect tests on three-points bending tests. Assuming a reliable description of the material non-linear behaviour at the global scale using a damage finite-element model, a re-analysis of the damage zone with a discrete-element model is performed. The global and the local results are both compared to the available experimental results and show a good agreement. The impact of the size effect on the cracking features is studied. Only the crack opening and the crack length have been studied here but some results about the micro-cracking area will be presented during the lecture. The experimental information about the micro-cracking area will be extracted from the DIC results as proposed by Skarzynski [10].

## REFERENCES

- [1] Bazant Z.P. and Plans J., 1998. Fracture and Size Effect in concrete and Other Quasi-brittle Materials. *CRC Press*.
- [2] Alam S.Y., Loukili A. and Grondin F., 2012. Monitoring size effect on crack opening in concrete by digital image correlation. *European Journal of Environmental and Civil Engineering*, **16:7**, 818-836.
- [3] Oliver-Leblond C., Delaplace A., Ragueneau F., and Richard B. Non-intrusive global/local analysis for the study of fine cracking. Submitted.
- [4] Delaplace A. and Desmorat R., 2007. Discrete 3D model as complimentary numerical testing for anisotropic damage. *Int. J. Fract.*, **148:6**, 115-128.
- [5] Richard B., Ragueneau F., Cremona C. and Adelaide L., 2010. Isotropic continuum damage mechanics for concrete under cyclic loading: Stiffness recovery, inelastic strains and frictional sliding. *Engineering Fracture Mechanics*, **77:8**, 1203-1223.
- [6] Van Mier J.G.M., Van Vliet M.R.A. and Wang T.K., 2002. Fracture mechanisms in particle composites: statistical aspects in lattice type analysis. *Mech. Mater.*, **34**, 705-724.
- [7] Voleti S.R., Chandra N. and Miller J.R., 1995. Global-local analysis of large-scale composite structures using finite element methods. *Comp. Struct.*, **58:3**, 453-464.
- [8] Pijaudier-Cabot G. and Bazant Z., 1987. Nonlocal damage theory. *Journal of Engineering Mechanics*, **1113**, 1512-1533.
- [9] Le Bellégo C., Dubé J.-F. and Pijaudier-Cabot G., 2003. Calibration of nonlocal damage model from size effect tests. *European Journal of Mechanics*, **22**, 33-46.
- [10] Skarzynski L., Syroka E. and Tejchman J., 2011. Measurements and Calculations of the Width of the Fracture Process Zones on the Surface of Notched Concrete Beams. *Strain*, **47**, 319-332.